Journal of Molecular Graphics and Modelling 29 (2010) 347–353

Contents lists available at ScienceDirect

Journal of Molecular Graphics and Modelling

journal homepage: www.elsevier.com/locate/JMGM

Molecular insight into the specific binding of ADP-ribose to the nsP3 macro domains of chikungunya and venezuelan equine encephalitis viruses: Molecular dynamics simulations and free energy calculations

Thanyada Rungrotmongkol[a,b,*], Nadtanet Nunthaboot[c], Maturos Malaisree[a], Nopporn Kaiyawet[a], Pathumwadee Yotmanee[a], Arthitaya Meeprasert[a], Supot Hannongbua[a]

[a] Computational Chemistry Unit Cell, Department of Chemistry, Faculty of Science, Chulalongkorn University, Bangkok 10330, Thailand
[b] Center of Innovative Nanotechnology, Chulalongkorn University, Bangkok 10330, Thailand
[c] Department of Chemistry, Faculty of Science, Mahasarakham University, Mahasarakham 44150 Thailand

ARTICLE INFO

Article history:
Received 16 July 2010
Received in revised form
19 September 2010
Accepted 23 September 2010
Available online 29 October 2010

Keywords:
Chikungunya
Venezuelan equine encephalitis
ADP-ribose
Molecular dynamics simulations

ABSTRACT

The outbreaks of chikungunya (CHIKV) and venezuelan equine encephalitis (VEEV) viral infections in humans have emerged or re-emerged in various countries of "Africa and southeast Asia", and "central and south America", respectively. At present, no drug or vaccine is available for the treatment and therapy of both viral infections, but the non-structural protein, nsP3, is a potential target for the design of potent inhibitors that fit at the adenosine-binding site of its macro domain. Here, so as to understand the fundamental basis of the particular interactions between the ADP-ribose bound to the nsP3 amino acid residues at the binding site, molecular dynamics simulations were applied. The results show that these two nsP3 domains share a similar binding pattern for accommodating the ADP-ribose. The ADP-ribose phosphate unit showed the highest degree of stabilization through hydrogen bond interactions with the nsP3 V33 residue and the consequent amino acid residues 110–114. The adenine base of ADP-ribose was specifically recognized by the conserved nsP3 residue D10. Additionally, the ribose and the diphosphate units were found to play more important roles in the CHIKV nsP3–ADP-ribose complex, while the ter-ribose was more important in the VEEV complex. The slightly higher binding affinity of ADP-ribose toward the nsP3 macro domain of VEEV, as predicted by the simulation results, is in good agreement with previous experimental data. These simulation results provide useful information to further assist in drug design and development for these two important viruses.

1. Introduction

Chikungunya (CHIKV) and Venezuelan equine encephalitis (VEEV) viruses are pathogens that are primarily transmitted to humans and/or animals through the bite of infected mosquitoes. With respect to, a diverse array of mosquito vectors exist, but species within the genus *Aedes* are the main vectors for both viruses, and in particular *A. aegypti*. The outbreaks of CHIKV in humans have been distributed in several countries of Africa and southeast Asia [1], while the VEEV outbreaks have occurred in the U.S.A., Mexico, Colombia and Venezuela [2]. Among the four non-structural (nsP1–4) and the main structural (capsids, E1 and E2) proteins encoded in their genomic RNA, the functions and the major role of the nsP3 protein are not yet clear, although the infection is required at an early stage in the transcription process for viral replication [3]. Here, an understanding at the atomic level of the molecular recognition and interaction between the ADP-ribose molecule and the nsP3 macro domain of CHIKV and VEEV, as model alphaviruses, is the main goal of this study. The simulated results constitute new important data to further assist in the design of inhibitors accommodating at the adenosine-binding site for the inhibition of these two alphaviruses.

CHIKV and VEEV viruses belong to the genus *Alphavirus* in the *Togaviridae* family. As with most other alphaviruses, they are enveloped, single stranded and positive sense RNA viruses. Their genomic RNA encodes for four non-structural proteins (nsP1–4) in the 5′ region and three main structural proteins (capsids, E1 and E2) in the 3′ region. The non-structural proteins have distinct important functions in the early stages of RNA replication, the negative strand synthesis [3–5]. In the latter stage of infection, the negative strand serves as a template for the synthesis of progeny-positive strands, and subgenomic mRNAs coding for the virus structural proteins.

* Corresponding author at: Computational Chemistry Unit Cell, Department of Chemistry, Faculty of Science, Chulalongkorn University, Bangkok, 10330, Thailand. Tel.: +66 22 187602; fax: +66 22 187603.
E-mail address: t.rungrotmongkol@gmail.com (T. Rungrotmongkol).

1093-3263/$ – see front matter © 2010 Elsevier Inc. All rights reserved.
doi:10.1016/j.jmgm.2010.09.010

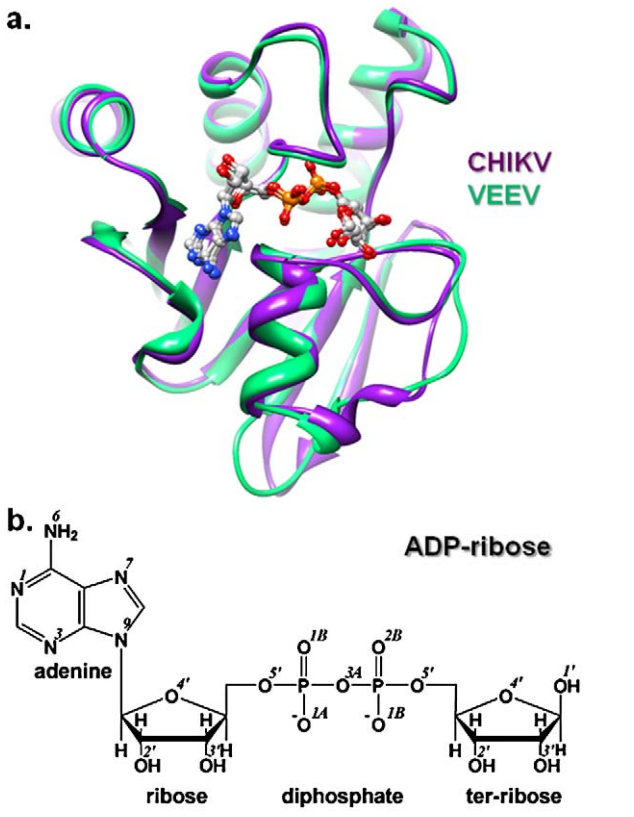

Fig. 1. (a) Structural alignment between the crystal structures of the CHIKV (violet) and VEEV (green) nsP3 macro domains complexed with ADP-ribose. (b) Schematic chemical structure of ADP-ribose containing adenine, ribose, diphosphate and ter-ribose moieties. (For interpretation of the references to color in this figure legend, the reader is referred to the web version of the article.)

The enzymatic machinery of three of the four non-structural proteins has been evaluated. The nsP1 protein is responsible for methylation and capping of viral mRNAs [6,7], directing the replication complex to the membrane [8], and association with the cytoplasmic surface of endosomes and lysosomes [9]. The nsP2 protein is a RNA triphosphatase [10], RNA helicase [11], NTPase [12] and protease [13]. The nsP4 protein is an RNA-dependent RNA polymerase involved in genome replication and transcription [14]. However, in some contrast, all that is known for the nsP3 protein is that it is proposed to be essential as a part of the minus strand replicase and mutations in it can reduce the rate of the minus strand and subgenomic RNA synthesis [15,16]. The nsP3 protein sequence is composed of three domains: (i) the C-terminal region with a poorly conserved sequence [17], (ii) the relatively well conserved serine/threonine rich sequence, and (iii) the N-terminal macro domain sequence. This macrodomain is ancient and is widely distributed throughout all eukaryotic organisms, bacteria and archaea [18]. Moreover, macro domains are also found in many types of positive strand RNA viruses, including hepatitis E, rubella, and those members of the corona- and alpha-viruses. The macro domain contains the binding domain for the ADP-ribose containing molecules: ADP-ribose, poly ADP-ribose and o-acetyl-ADP-ribose [19–22]. Recently, the crystal structures of the nsP3 macro domain for the VEEV and CHIKV have been reported (Fig. 1a) [23]. Each domain contains the six-stranded β sheet with three α helices. The intermolecular interactions between the residues in the binding pocket of the two enzymes and the ADP-ribose, as analyzed from their crystal structures, are drawn in Fig. 2.

To gain the fundamental knowledge on the structure and binding modes of ADP-ribose in the nsP3 macro domains of CHIKV and

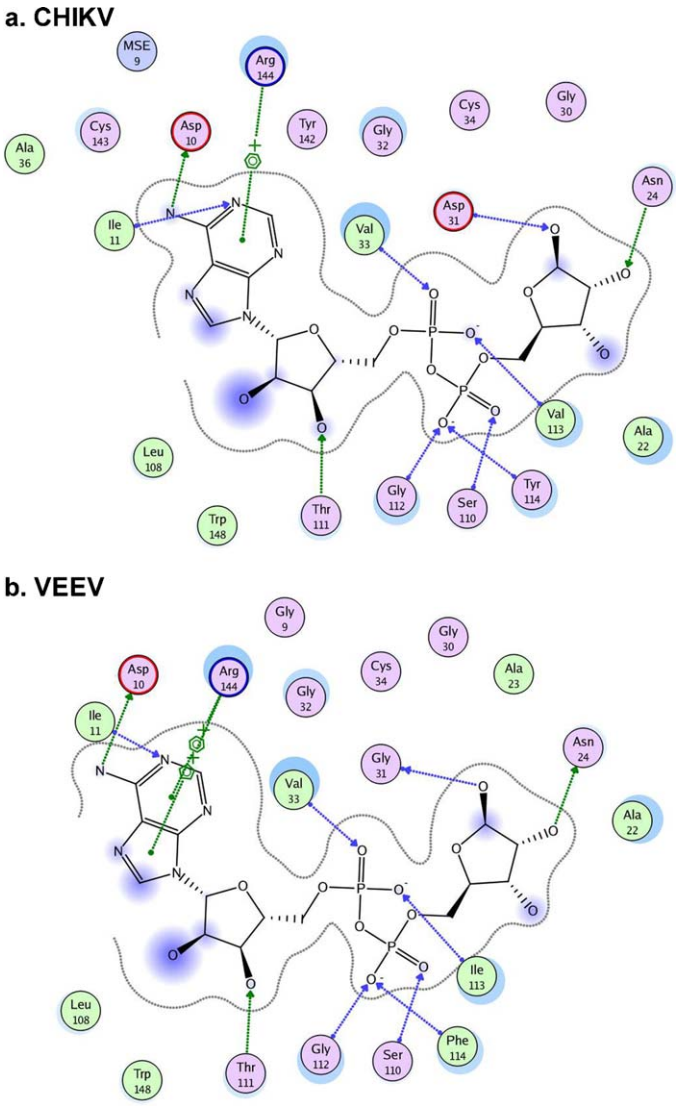

Fig. 2. Schematic representations on intermolecular interactions between ADP-ribose and the residues at the binding pocket of the nsP3 macro domains of (a) CHIKV and (b) VEEV, based on the crystal structures [23].

VEEV in aqueous solution, molecular dynamics (MD) simulations of the ADP-ribose bound with both CHIKV and VEEV macro domains were conducted. The results were extensively analyzed in terms of intermolecular hydrogen bonds, decomposition free energy and its components, and the binding free energy of the complex focused on the ADP-ribose binding pocket.

2. Materials and methods

2.1. System preparation

The recently reported X-ray crystallographic structures of the CHIKV and VEEV nsP3 macro domains complexed with the ADP-ribose [23] (Fig. 1a), taken from the Protein Data Bank (PDB) (entry codes 3GPO and 3GQO, respectively), were used as the starting coordinates for the MD simulations. Initial structure preparations and calculation processes were carried out using the AMBER package suit of programs [24]. The AMBER ff03 force field [25] was applied for amino acid residues while the ADP parameters [26] were used to create the parameters for ADP-ribose. Likewise the protonation states for the five ionizable amino acids (Asp, Glu, Lys, Arg and His) were assigned using the PROPKA program [27].

All missing hydrogen atoms of the proteins and ADP-ribose were added with standard bond lengths and angles by the LEaP module of AMBER. To relieve bad steric interactions, the hydrogen atoms were firstly minimized with 1500 steps of steepest descents (SD) followed by 1500 steps of conjugated gradient (CG). Afterwards, each complex was immersed in a cubic box of TIP3P water molecules [28] and, in the case of CHIKV, a sodium counterion was randomly added to neutralize the electrical charge of the CHIKV. The number of total atoms and the water box size of the CHIKV system were 25,893 atoms and $66 \times 67 \times 74$ Å^3, while those for the VEEV complex were 24,588 atoms and $65 \times 68 \times 69$ Å^3, respectively. Based on a cutoff distance of 12 Å, the added water molecules were consequently energy minimized using 1500 steps each of SD and CG, while the protein and ligand were restrained with a force constant of 500 kcal/molÅ^2. Finally, the entire structure was fully minimized with 3000 steps each for SD and CG, to search for the optimum conformation.

2.2. Molecular dynamics simulations

All simulations were carried out under the periodic boundary condition with the *NPT* ensemble. The SHAKE algorithm [29] was applied to constrain all covalent bonds involving hydrogen atoms. A time step of 2 fs with residue-based non-bonded interactions truncated at 12 Å was used. The long-range electrostatic interactions [30] were calculated according to the particle mesh Ewald method. A Berendsen coupling time of 0.2 ps was employed to maintain the temperature and standard pressure of the system [31]. Firstly, both complexes were heated up to 298 K for 60 ps. Then, the MD simulations were performed for 10 ns, consisting of the first 4 ns of equilibration and another 6 ns of the production phase. The trajectories, collected every 0.2 ps in the production phase, were used for analysis.

The convergences of energy, temperature, pressure and the global root mean-square displacement (RMSD) were used to verify the system stability. The MD trajectories extracted from the production phase were analyzed in terms of hydrogen bond (H-bond), decomposition of free energies on a per-residue basis ($\Delta G_{bind}^{residue}$), binding free energies (ΔG_{bind}) and their energy components.

2.3. Molecular mechanics/Poisson–Boltzmann Surface Area (MM/PBSA) calculations

The Molecular Mechanics/Poisson–Boltzmann Surface Area (MM/PBSA) approach is a well-accepted method to estimate the binding free energy between a protein and its given ligand [32–34]. This method, as implemented in the AMBER program, was applied to compute the binding free energies for the CHIKV and VEEV nsP3 macro domain complexed with ADP-ribose. Here, changes in the binding free energy in the protein (nsP3 macro domain)–ligand (ADP-ribose) binding is computed as the difference between the free energies of the complex ($\Delta G_{complex}$), protein (ΔG_{ligand}) and ligand (ΔG_{ligand}), as outlined in Eq. (1):

$$\Delta G_{bind} = \Delta G_{complex} - [\Delta G_{protein} + \Delta G_{lig}] \quad (1)$$

In general, the total free energy of each species contains the enthalpy and entropy contributions, as shown in Eq. (2):

$$\Delta G = \Delta H - T\Delta S \quad (2)$$

where ΔH of the system is composed of the enthalpy changes in the gas phase upon complex formation (ΔE_{MM}) and the solvated free energy contribution (ΔG_{sol}), while $-T\Delta S$ refers to the entropy contribution to the binding. Eq. (2) can be then approximated as shown in Eq. (3):

$$\Delta G = \Delta E_{MM} + \Delta G_{sol} - T\Delta S \quad (3)$$

where ΔE_{MM} is the summation of the van der Waals (ΔE_{vdW}) and the electrostatic (ΔE_{ele}) interaction energies, and was evaluated by the SANDER module of AMBER using Eq. (4):

$$\Delta E_{MM} = \Delta E_{vdW} + \Delta E_{ele} \quad (4)$$

In addition, ΔG_{sol}, which denotes the solvation free energy, can be computed as the summation of an electrostatic component ($\Delta G_{ele,sol}$) and a nonpolar component ($\Delta G_{nonpolar,sol}$), as shown in Eq. (5):

$$\Delta G_{sol} = \Delta G_{ele,sol} + \Delta G_{nonpolar,sol} \quad (5)$$

The electrostatic component was computed by the Possion-Boltzmann (PB) method [35,36] in the AMBER suite. The dielectric constants for the solute and the surrounding solvent were set to 1 and 80, respectively. The same set of atomic charges on each complex applied in the MD simulations was again used in the PB computation. The nonpolar term in the solvation free energy was computed, as shown in Eq. (6):

$$\Delta G_{nonpolar,sol} = \gamma SASA + \beta \quad (6)$$

where *SASA* is the solvent accessible surface area of each given molecule and is determined using a solvent probe radius of 1.4 Å. For the PB model, the values of the surface tension constants γ and β were set to 0.0072 kcal/mol Å^2 and 0.00 kcal/mol, respectively. The entropy term $T\Delta S$ is required to account for the conformational entropy change of the two binding partners upon complexation. In this study, we performed a normal-mode analysis [37], using the NMODE module, to compute the vibrational, rotational and translational entropies.

2.4. Binding free energy decomposition

The contribution of each residue to the total binding free energy of the protein–ligand complex, according to Eq. (1), was evaluated through the free energy decomposition based on the MM/PBSA method [38,39]. For this purpose, the contribution of atom *i* to the total electrostatic interaction energy between the two components is given by one half of a pairwise electrostatic interaction energy between the two atoms, each belonging to the protein and ligand complex. This is expressed in Eq. (7) as:

$$E_{ele}^{i} = \frac{1}{2}\sum_{j \neq i} \frac{q_i q_j}{r_{ij}} \quad (7)$$

where *j* are the atoms of the part that *i* does not belong to, whereas r_{ij} is the distance between the two atoms with atomic partial charges of q_i and q_j. Similarly, one half of the pairwise intercomponent van der Waals interaction energies (E_{vdW}^{i}) between the nsP3 protein and the ADP-ribose ligand was attributed to avoid double counting. The calculation of the internal energy, ΔE_{int}, is equal to zero under the assumption of a single trajectory approach since the internal energies of the complex and the separated parts are calculated from the same trajectory. The *SASA* of each atom *i* to the nonpolar solvation term is given by Eq. (8):

$$\Delta G_{nonpolar,sol}^{i} = \gamma \times (SASA^{i,complex} - (SASA^{i,protein} + SASA^{i,ligand})) \quad (8)$$

where $SASA^{i,protein}$ or $SASA^{i,ligand}$ is equal to zero depending on which component the atom belongs to. The GB approach was used to calculate electrostatic free energy term by Eq. (9):

$$\Delta G_{ele,sol} = -\frac{1}{2}\left(1 - \frac{e_{GB}^{-\kappa f}}{\varepsilon_{\omega}}\right)\sum_{ij}\frac{q_i q_j}{f_{GB}} \quad (9)$$

where ε_{ω} is the dielectric constant of solvent, κ is the Debye–Hückel screening parameter and the double sum runs over all pairs of

atoms. In this study, ε_ω and κ were assigned to 80 and 0, respectively, and f_{GB} was defined by Eq. (10):

$$f_{GB} = \left[r_{ij}^2 + \alpha_i \alpha_j \exp\left(\frac{-r_{ij}^2}{4\alpha_i \alpha_j} \right) \right]^{1/2} \quad (10)$$

where α_i and α_j are the effective Born radius of atoms i and j, respectively. The contribution of atom i to the electrostatic free energy is obtained by Eq. (11):

$$\Delta G^i_{ele,sol} = -\frac{1}{2} \sum_j \left(1 - \frac{e^{-\kappa f}}{\varepsilon_\omega} \right) \frac{q_i q_j}{f_{GB_{ij}}(r_{ij})} + \frac{1}{2} \sum_{j \neq i} \frac{q_i q_j}{r_{ij}} \quad (11)$$

Finally, the contribution to the total binding free energy for a per-residue basis, $\Delta G^{residue}_{bind}$, can be obtained by summation of the atomic contributions E^i_{ele}, E^i_{vdW}, $\Delta G^i_{ele,sol}$ and $\Delta G^i_{nonpolar,sol}$ over the atoms of a given residue without consideration of the entropy terms. The separated contribution of its backbone, $\Delta G^{backbone}_{bind}$, or the side chain, $\Delta G^{side\ chain}_{bind}$, can be constructed from the related atoms.

3. Results and discussion

To determine the system stability of the CHIKV and VEEV nsP3–ADP-ribose complexes, RMSDs of the heavy atoms over 10-ns MD simulation with respect to their starting structures were plotted versus simulation time and given in Fig. S1 (see supplementary data). It can be seen that the two complexes were found to reach equilibrium at 4-ns and thus the MD trajectories taken from the subsequent 6-ns simulations were properly used for analysis.

3.1. Key binding motif of ADP-ribose

To obtain detailed information and insight into the intermolecular interactions of the ADP-ribose and the nsP3 protein, the percentage and the number of hydrogen bond (H-bond) occupations between the ADP-ribose and the binding residues of the CHIKV and the VEEV nsP3 macro domains were identified according to the subsequent criteria: (i) the distance between proton donor (D) and acceptor (A) atoms ≤ 3.5 Å; and (ii) the D–H$\cdots$A angle ≥ 120. The results are summarized in Fig. 3, where the strong and medium hydrogen bond interactions are determined by H-bond occupations of higher than 75% and 50%, respectively (dashed lines in Fig. 3). We assume that the strongly detected H-bonds at the binding site of the nsP3 macro domain could provide the important interactions between the binding pocket residues and the ADP-ribose molecule.

The stabilization at the adenine base of ADP-ribose in both viral nsP3–ADP-ribose complexes was mostly contributed from the nsP3 residues D10 and I11. The backbone nitrogen of I11 stabilized the ribose through a very strong hydrogen bond with the N^1-nitrogen (see atomic label in Fig. 1b), which is in good agreement with the schematic view of the protein–ligand interactions determined from the X-ray structures (Fig. 2). Its N^6-nitrogen established two moderate strength hydrogen bond interactions with the two carboxylate oxygens of D10, while in the crystal structures [23] only the hydrogen bond with the O^{D1}-oxygen of D10 (3.0 Å in CHIKV and 2.7 Å in VEEV) was formed. In addition, it was proposed that the high specificity of the adenine moiety of ADP-ribose in the binding to the alphavirus CHIKV and VEEV nsP3 macro domains was mainly achieved through the conserved residue D10 [23]. A significant decrease in the protein thermal stability for the GDP binding to the CHIKV nsP3 macro domain, compared to that of the ADP–protein complex [23], is most likely caused by a lack of any particular interaction between the nsP3 D10 residue and the GDP guanine base.

By considering the interaction of the connecting ribose (Fig. 3), although the two simulated models exhibited a similar strong hydrogen bond between their $O^{3'}$-hydroxyl oxygen of the ribose and the hydroxyl moiety of the nsP3 T111 residue, the interaction to the R144 residue was significantly different. In the case of CHIKV, the ribose $O^{2'}$-hydroxyl oxygen was intensely stabilized by the nsP3 R144 residue through the presence of two strong hydrogen bonds with the gaunidinium group at the N^E- and N^{H2}-nitrogens. In contrast, these interactions had almost disappeared in the case of the VEEV nsP3–ADP-ribose complex where only a very weak hydrogen bond with one of the gaunidinium nitrogen's of the R144 residue was observed.

Both the CHIKV and the VEEV nsP3–ADP-ribose complexes shared relatively similar patterns of hydrogen bond interactions at the diphosphate unit (Fig. 3). There was a strong hydrogen bond between the O^{1A}-phosphate oxygen and the backbone nitrogen of the nsP3 V33 residue. The O^{1B}- and O^{2B}-phosphate oxygens established strong and rather weak hydrogen bonds, respectively, to the backbone nitrogen of S110. Furthermore, the O^{2B} atom formed two strong hydrogen bonds, one each with residues G112 and either Y114 (CHIKV) or F114 (VEEV). However, a clear difference between the two viral nsP3–ADP-ribose complexes was found in terms of the interaction with residue 133. In CHIKV, two strong hydrogen bonds were formed between the two phosphate oxygens (O^{2A} and O^{2B}) of the ADP-ribose and the backbone of the nsP3 residue V113, whereas one of these interactions was weaker at the I113 residue in the VEEV nsP3–ADP-ribose complex.

Moreover, interactions between the ADP-ribose and the two viral nsP3 macro domains are remarkably different at the ter-ribose unit. Only one strong hydrogen bond was found between the $O^{5'}$-phosphate connecting oxygen and the backbone nitrogen of the nsP3 Y114 residue in CHIKV (Fig. 3a), while three strong hydrogen bonds to nsP3 residues G31, G32 and F114 were detected in the VEEV nsP3–ADP-ribose complex (Fig. 3b). Conversion of the D31 residue to G31 in the VEEV nsP3 protein leads to the formation of a strong hydrogen bond between the G31 residue and the ter-ribose unit, instead of the two moderate hydrogen bonds seen with the D31 residue through its backbone oxygen and nitrogen atoms as observed in CHIKV. This was subsequently found to affect the adjacent residue where the interaction with G32 in the case of the VEEV nsP3–ADP-ribose complex is markedly stronger than that in the CHIKV case. The $O^{5'}$ atom of the ter-ribose moiety made a stronger hydrogen bond to the nsP3 I113 residue in VEEV than with the V113 residue in CHIKV. Furthermore, the H-bond between the nitrogen backbone of the nsP3 residue Y114 (CHIKV) or F114 (VEEV) and the $O^{5'}$ atom of the ADP-ribose unit was well conserved.

Taking into account all of the above information, the hydrogen bond patterns between the ADP-ribose and the nsP3 macro domains for both CHIKV and VEEV are almost the same. The nsP3 amino acid residues D10, I11, N24, D/G31-C34, S110-Y/F114 and R144 were found to be the key residues for the enzyme-ligand binding. In addition, the ribose and diphosphate units of the ADP-ribose were found to play more important roles in the CHIKV nsP3–ADP-ribose complex, while the strongly stabilized ter-ribose played the main part in the VEEV nsP3–ADP-ribose complex.

3.2. Per residue nsP3 enzyme–ADP-ribose interactions

To provide the basic information on the intermolecular interactions contributed from the individual residues in the CHIKV and VEEV nsP3 macro domains to the ADP-ribose, the pair interaction decomposition of free energy ($\Delta G^{residue}_{bind}$, the per residue total binding free energy) was evaluated using the decomposition energy module in AMBER. The calculation was performed over the 100 MD snapshots taken from the last 6-ns simulation. The summations

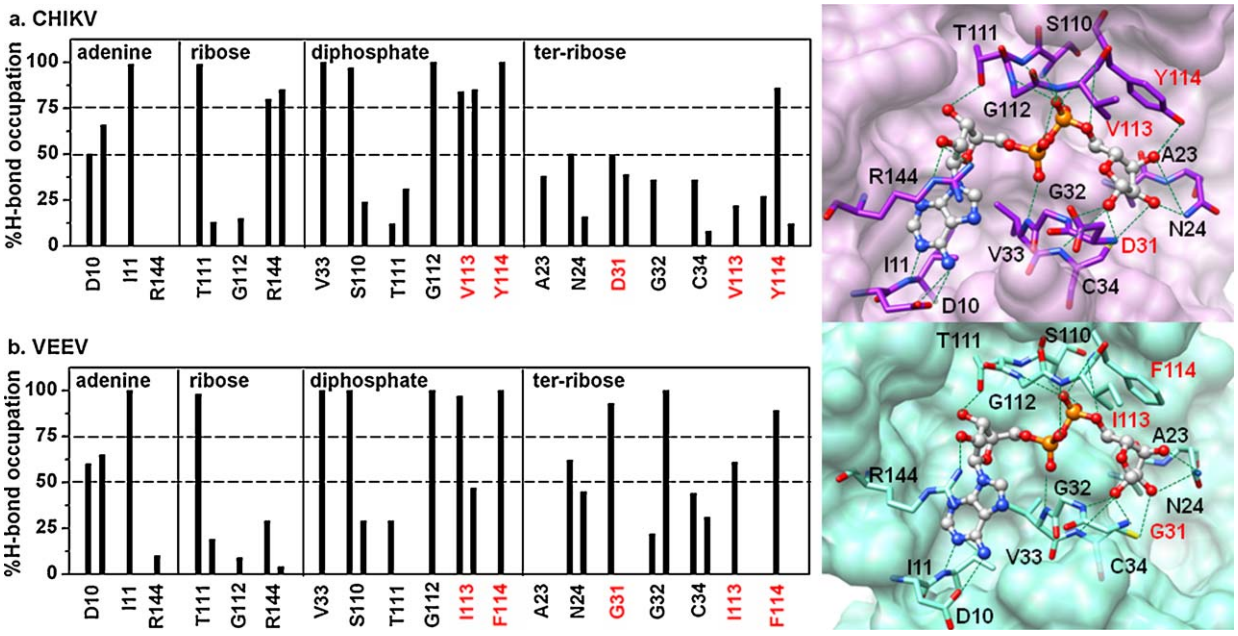

Fig. 3. Left: Percentage occupation of H-bonds between each ADP-ribose moiety (see Fig. 1b for definition) and the key residues in the binding pocket of the (a) CHIKV and (b) VEEV nsP3 macro domains. Right: The schematic view of the ADP-ribose (ligand)-nsP3 protein interaction, taken from the last MD snapshot is also depicted for both viruses, where the nsP3 residues that are different between the two macro domains are shown in red.

of per residue interaction free energies were separated into the residue backbone ($\Delta G_{bind}^{backbone}$) and the side chain ($\Delta G_{bind}^{side\ chain}$). The energy contributions from the selected residues are summarized in Fig. 4.

As shown, the plots for both viral nsP3–ADP-ribose systems show similar trends and almost the same patterns of decomposition energies (Fig. 4). The major contribution to the binding mode of the ADP-ribose, with a $\Delta G_{bind}^{residue}$ of ≤ -4 kcal/mol (black column), was obviously gained from the many key nsP3 amino acid residues located in the ADP-ribose binding pocket of the CHIKV and VEEV macro domains. These residues are G32, V33, L109 (VEEV), S110, T111, G112, V133 (CHIKV) or I113 (VEEV), Y114 (CHIKV) or F114 (VEEV), and R144 (CHIKV), which directly face to the diphosphate moiety of ADP-ribose (see schematic view in Fig. 3). Based on this major contribution, with a $\Delta G_{bind}^{residue}$ of ≤ -4 kcal/mol, the energy contribution to the ADP-ribose molecule in VEEV (Fig. 4b) is slightly larger than that for CHIKV (Fig. 4a). In both systems, the interactions of these key residues were mainly achieved from their backbone atoms (light grey column, Fig. 4), which are in good agreement with the formation of many H-bonds with the backbone nitrogen and oxygen atoms, as previously mentioned above. Additionally, an essential contribution to the binding energy in the range of $-4 \leq \Delta G_{bind}^{residue} \leq -2$ kcal/mol was provided by the four nsP3 amino acid residues (I11, A22, N24 and L109) in CHIKV, and the six residues (I11, A22, N24, G30, G31 and C34) in VEEV.

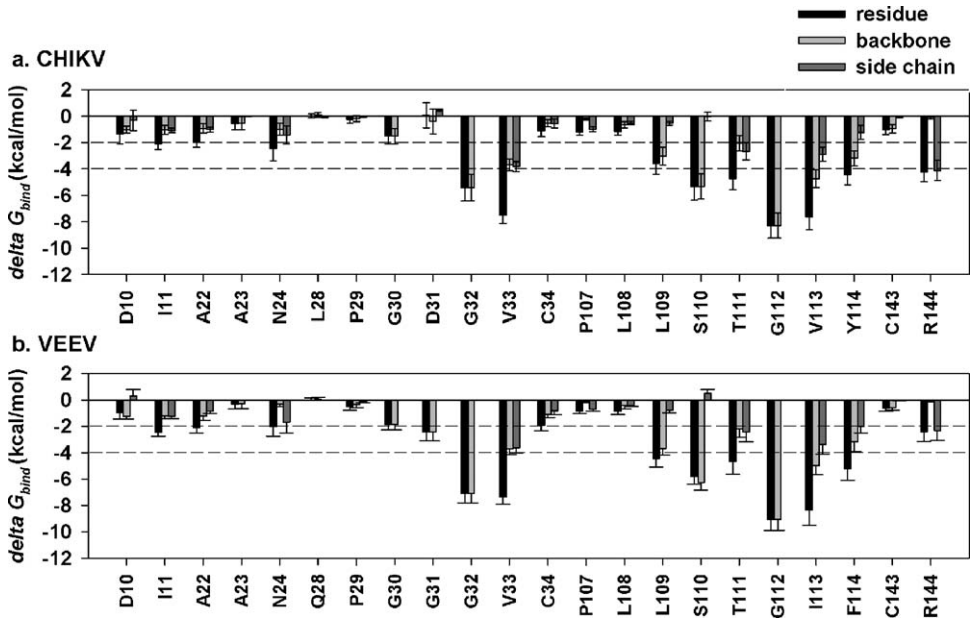

Fig. 4. Decomposition of the free energy on a per-residue basis ($\Delta G_{bind}^{residue}$) into the contributions from the atom groups of the backbone ($\Delta G_{bind}^{backbone}$) and the side chain ($\Delta G_{bind}^{side\ chain}$) in the (a) CHIKV and (b) VEEV nsP3 macro domains bound to ADP-ribose.

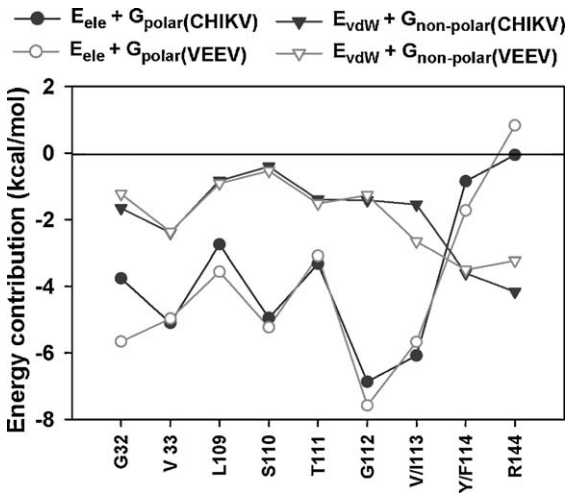

Fig. 5. Energy contribution of electrostatic and van der Waals terms for the key residues of the two nsP3 protein macro domains, CHIKV and VEEV.

To reveal the source of the interaction contribution from each particular residue, the electrostatic ($E_{ele} + G_{polar}$) and van der Waals ($E_{vdW} + G_{nonpolar}$) energy terms of the nine key residues in both alphaviruses were plotted and compared (Fig. 5). Except for the residues Y114 (CHIKV) or F114 (VEEV) and R144, the majority of the decomposed energy interaction originated from the electrostatic contribution apparently through H-bonding interactions, while the van der Waals contribution appeared as a minor influence to those key residues in the ADP-ribose binding process.

3.3. Binding affinity of ADP-ribose

The total binding free energy for the ADP-ribose molecule, ΔG_{bind}, and its detailed energy contributions calculated according to the MM/PBSA approach, are summarized in Table 1. Note that the 100 MD snapshots used in the MM/PBSA calculations were the same set as those used to evaluate the pair interaction decomposition of free energy. The ΔG_{bind} can be divided into polar ($E_{vdW} + G_{nonpolar}$) and nonpolar ($\Delta G_{nonpolar,sol} + \Delta E_{vdW}$) energies, whereupon the free energy of the ADP-ribose binding is revealed to be primarily contributed from the $\Delta G_{nonpolar,sol} + \Delta E_{vdW}$ at −72.6 and −71.8 kcal/mol for the CHIKV and VEEV, respectively, while the $\Delta G_{ele,sol} + \Delta E_{ele}$ shows a likely unfavorable contribution at 36.8 and 32.5 kcal/mol for the CHIKV and VEEV, respectively. In the latter case, this is due to the intermolecular electrostatic energy, which is mainly achieved from the many hydrogen bond formations with the ADP-ribose binding residues of the nsP3 macro domain (as discussed above), and is lower than the desolvation energy. This occurrence has been reported in the previous theoretical studies of the interactions and binding free energies between ligands and proteins in an aqueous solution [40–43]. With the summation of the solute entropy term (∼30 kcal/mol), an estimated ΔG_{bind} of −6.2 kcal/mol and −9.0 kcal/mol was found for the CHIKV and VEEV complexes, respectively, suggesting that the ADP-ribose binds to and interacts with the binding site of the VEEV nsP3 macro domain slightly stronger than that with CHIKV. These simulation based results are in a good agreement with the experimental dissociation constant (K_d) of ADP-ribose binding to the nsP3 macro domain of these two alphaviruses [23].

Table 1
Calculated energy components, binding free energy (kcal/mol) and experimental dissociation constant (K_d, μM) of ADP-ribose binding to macro domain of (a) CHIKV and (b) VEEV.

	CHIKV	VEEV
ΔE_{ele}	−316.8 ± 22.0	−376.8 ± 16.7
ΔE_{vdW}	−64.9 ± 4.3	−64.5 ± 3.7
ΔE_{MM}	−381.7 ± 22.7	−441.3 ± 17.1
$\Delta G_{nonpolar,sol}$	−7.7 ± 0.2	−7.3 ± 0.2
$\Delta G_{ele,sol}$	353.6 ± 20.8	409.4 ± 14.9
ΔG_{sol}	345.8 ± 20.9	402.0 ± 14.9
$\Delta G_{ele,sol} + \Delta E_{ele}$	36.8 ± 8.2	32.5 ± 7.3
$\Delta G_{nonpolar,sol} + \Delta E_{vdW}$	−72.6 ± 2.3	−71.8 ± 2.0
ΔG_{total}	−35.9 ± 7.1	−39.3 ± 6.4
$-T\Delta S$	29.7 ± 3.5	30.3 ± 2.1
ΔG_{bind}	−6.2 ± 5.6	−9.0 ± 4.8
K_d (μM) [23]	5 ± 0.4	3.9 ± 0.65

4. Conclusions

In this study, molecular dynamics simulations were used to identify the key residues at the ADP-ribose binding site of the CHIKV and NEEV nsP3 macro domains for the design of potent inhibitors against these viruses. The likely binding motif for the ADP-ribose in both nsP3 enzyme targets was found to be considerably similar, involving the potential binding residues of D10, I11, N24 and R144, D/G31-C34, and S110-Y/F114. Among the four subunits of the ADP-ribose, the negatively charged PO_4^{2-} moiety showed the strongest interactions with the above residues in the binding pocket of enzyme. In addition, the ribose and the diphosphate units were found to play more important roles in the CHIKV nsP3–ADP-ribose complex, while the ter-ribose moiety was more important in the corresponding VEEV complex. The per-residue decomposition energies suggested that the particular interactions between the ADP-ribose and the nsP3 macro domain were mostly derived from the electrostatic contributions, apparently through hydrogen bond interactions with the residue backbone. In addition, the binding efficiency of the ADP-ribose towards the nsP3 macro domain of CHIKV was predicted to be slightly lower than that for VEEV, which concurs with the experimental data. An understanding of the specific interactions between the ADP-ribose and the nsP3 macro domain at the molecular level is useful information to further assist in drug design and development for these two important viruses.

Acknowledgments

This work was supported by The Thailand Research Fund, and the Thai Government Stimulus Package 2 (TKK2555), under the Project for Establishment of Comprehensive Center for Innovative Food, Health Products and Agriculture. T.R. thanks the Ratchadaphiseksomphot Endowment Fund from Chulalongkorn University for Postdoctoral fellowship, and the TRF Grant for New Research (Grant No. TRG5280035). The Computational Chemistry Unit Cell at Chulalongkorn University provided the computing facilities. The Center of Excellence for Petroleum, Petrochemicals and Advanced Materials, Chulalongkorn University, is acknowledged.

Appendix A. Supplementary data

Supplementary data associated with this article can be found, in the online version, at doi:10.1016/j.jmgm.2010.09.010.

References

[1] S.K. Lam, K.B. Chua, P.S. Hooi, M.A. Rahimah, S. Kumari, M. Tharmaratnam, S.K. Chuah, D.W. Smith, I.A. Sampson, Chikungunya infection—an emerging disease in Malaysia, Southeast Asian J. Trop. Med. Public Health 32 (2001) 447–451.
[2] J.G. Estrada-Franco, R. Navarro-Lopez, J.E. Freier, D. Cordova, T. Clements, A. Moncayo, W. Kang, C. Gomez-Hernandez, G. Rodriguez-Dominguez, G.V. Ludwig, S.C. Weaver, Venezuelan equine encephalitis virus, southern Mexico, Emerg. Infect. Dis. 10 (2004) 2113–2121.
[3] Y.F. Wang, S.G. Sawicki, D.L. Sawicki, Alphavirus nsP3 functions to form replication complexes transcribing negative-strand RNA, J. Virol. 68 (1994) 6466–6475.

[4] J.A. Lemm, T. Rümenapf, E.G. Strauss, J.H. Strauss, C.M. Rice, Polypeptide requirements for assembly of functional Sindbis virus replication complexes: a model for the temporal regulation of minus- and plus-strand RNA synthesis, EMBO J. 13 (1994) 2925–2934.
[5] Y. Shirako, J.H. Strauss, Regulation of Sindbis virus RNA replication: uncleaved P123 and nsP4 function in minus-strand RNA synthesis, whereas cleaved products from P123 are required for efficient plus-strand RNA synthesis, J. Virol. 68 (1994) 1874–1885.
[6] P. Laakkonen, M. Hyvönen, J. Peränen, L. Kääriäinen, Expression of Semliki Forest virus nsP1-specific methyltransferase in insect cells and in *Escherichia coli*, J. Virol. 68 (1994) 7418–7425.
[7] T. Ahola, L. Kääriäinen, Reaction in alphavirus mRNA capping: formation of a covalent complex of nonstructural protein nsP1 with 7-methyl-GMP, Proc. Natl. Acad. Sci. U.S.A. 92 (1995) 507–511.
[8] T. Ahola, A. Lampio, P. Auvinen, L. Kääriäinen, Semliki Forest virus mRNA capping enzyme requires association with anionic membrane phospholipids for activity, EMBO J. 18 (1999) 3164–3172.
[9] J. Peränen, P. Laakkonen, M. Hyvönen, L. Kääriäinen, The alphavirus replicase protein nsP1 is membrane-associated and has affinity to endocytic organelles, Virology 208 (1995) 610–620.
[10] L. Vasiljeva, A. Merits, P. Auvinen, L. Kääriäinen, Identification of a novel function of the alphavirus capping apparatus RNA 5′-triphosphatase activity of nsP2, J. Biol. Chem. 275 (2000) 17281–17287.
[11] M. Gomez de Cedróna, N. Ehsani, M.L. Mikkola, J.A. Garcıĭaa, L. Kääriäinen, RNA helicase activity of Semliki Forest virus replicase protein nsP2, FEBS Lett. 448 (1999) 19–22.
[12] D.L. Sawicki, S. Perri, J.M. Polo, S.G. Sawicki, Role for nsP2 proteins in the cessation of alphavirus minus-strand synthesis by host cells, J. Virol. 80 (2006) 360–371.
[13] D.J. Barton, S.G. Sawicki, D.L. Sawicki, Demonstration in vitro of temperature-sensitive elongation of RNA in Sindbis virus mutant ts6, J. Virol. 62 (1988) 3597–3602.
[14] J.K. Rubach, B.R. Wasik, J.C. Rupp, R.J. Kuhn, R.W. Hardy, D.W. Smith, Characterization of purified Sindbis virus nsP4 RNA-dependent RNA polymerase activity in vitro, Virology 384 (2009) 201–208.
[15] I. De, C. Fata-Hartley, S.G. Sawicki, D.L. Sawicki, Functional analysis of nsP3 phosphoprotein mutants of Sindbis virus, J. Virol. 77 (2003) 13106–13116.
[16] M.W. LaStarza, J.A. Lemm, C.M. Rice, Genetic analysis of the nsP3 region of Sindbis virus: evidence for roles in minus-strand and subgenomic RNA synthesis, J. Virol. 68 (1994) 5781–5791.
[17] J.H. Strauss, E.G. Strauss, The alphaviruses: gene expression, replication, and evolution, Microbiol. Rev. 58 (1994) 491–562.
[18] J.R. Pehrson, R.N. Fuji, Evolutionary conservation of histone macroH2A subtypes and domains, Nucleic Acids Res. 26 (1998) 2837–2842.
[19] L.R. Comstock, J.M. Denu, Synthesis and biochemical evaluation of *O*-acetyl-ADP-ribose and *N*-acetyl analogs, Org. Biomol. Chem. 5 (2007) 3087–3091.
[20] M.P. Egloff, H. Malet, A. Putics, M. Heinonen, H. Dutartre, A. Frangeul, A. Gruez, V. Campanacci, C. Cambillau, J. Ziebuhr, T. Ahola, B. Canard, Structural and functional basis for ADP-ribose and poly(ADP-ribose) binding by viral macro domains, J. Virol. 80 (2006) 8493–8502.
[21] G.I. Karras, G. Kustatscher, H.R. Buhecha, M.D. Allen, C. Pugieux, F. Sait, M. Bycroft, A.G. Ladurner, The macro domain is an ADP-ribose binding module, EMBO J. 24 (2005) 1911–1920.
[22] G. Kustatscher, M. Hothorn, C. Pugieux, K. Scheffzek, A.G. Ladurner, Splicing regulates NAD metabolite binding to histone macroH2A, Nat. Struct. Mol. Biol. 12 (2005) 624–625.
[23] H. Malet, B. Coutard, S. Jamal, H. Dutartre, N. Papageorgiou, M. Neuvonen, T. Ahola, N. Forrester, E.A. Gould, D. Lafitte, F. Ferron, J. Lescar, A.E. Gorbalenya, X. de Lamballerie, B. Canard, The crystal structures of Chikungunya and Venezuelan equine encephalitis virus nsP3 macro domains define a conserved adenosine binding pocket, J. Virol. 83 (2009) 6534–6545.
[24] D.A. Case, T.A. Darden, T.E.I. Cheatham, C.L. Simmerling, J. Wang, R.E. Duke, R. Luo, W. Crowley, R.C. Walker, W. Zhang, K.M. Merz, B. Wang, S. Hayik, A. Roitberg, G. Seabra, I. Kolossváry, K.F. Wong, F. Paesani, J. Vanicek, X. Wu, S.R. Brozell, T. Steinbrecher, H. Gohlke, L. Yang, C. Tan, J. Mongan, V. Hornak, G. Cui, D.H. Mathews, M.G. Seein, C. Sagui, V. Babin, P.A. Kollman, AMBER 10 (2008).
[25] Y. Duan, C. Wu, S. Chowdhury, M.C. Lee, G. Xiong, W. Zhang, R. Yang, P. Cieplak, R. Luo, T. Lee, J. Caldwell, J. Wang, P. Kollman, A point-charge force field for molecular mechanics simulations of proteins based on condensed-phase quantum mechanical calculations, J. Comput. Chem. 24 (2003) 1999–2012.
[26] K.L. Meagher, L.T. Redman, H.A. Carlson, Development of polyphosphate parameters for use with the AMBER force field, J. Comput. Chem. 24 (2003) 1016–1025.
[27] H. Li, A.D. Robertson, J.H. Jensen, Very fast empirical prediction and rationalization of protein p*K*a values, Proteins 61 (2005) 704–721.
[28] W.L. Jorgensen, J. Chandrasekhar, J.D. Madura, R.W. Impey, M.L. Klein, Comparison of simple potential functions for simulating liquid water, J. Chem. Phys. 79 (1983) 926–935.
[29] J.P. Ryckaert, G. Ciccotti, H.J.C. Berendsen, Numerical integration of the Cartesian equations of motion of a system with constraints: molecular dynamics of n-alkanes, J. Comput. Phys. 23 (1997) 327–341.
[30] D.M. York, T.A. Darden, L.G. Pedersen, The effect of long-range electrostatic interactions in simulations of macromolecular crystals: a comparison of the Ewald and truncated list methods, J. Chem. Phys. 99 (1993) 8345–8348.
[31] H.J.C. Berendsen, J.P.M. Postma, W.F.V. Gunsteren, A. DiNola, Molecular dynamics with coupling to an external bath, J. Chem. Phys. 81 (1984) 3684–3690.
[32] M. Malaisree, T. Rungrotmongkol, P. Decha, P. Intharathep, O. Aruksakunwong, S. Hannongbua, Understanding of known drug-target interactions in the catalytic pocket of neuraminidase subtype N1, Proteins 71 (2008) 1908–1918.
[33] P.A. Kollman, I. Massova, C. Reyes, B. Kuhn, S. Huo, L. Chong, M. Lee, T. Lee, Y. Duan, W. Wang, O. Donini, P. Cieplak, J. Srinivasan, D.A. Case, T.E. Cheatham, Calculating structures and free energies of complex molecules: combining molecular mechanics and continuum models, Acc. Chem. Res. 33 (2000) 889–897.
[34] J. Srinivasan, T.E. Cheatham, P. Cieplak, P.A. Kollman, D.A. Case, Continuum solvent studies of the stability of DNA RNA, and phosphoramidate—DNA helices, J. Am. Chem. Soc. 120 (1998) 9401–9409.
[35] G. Lamm, Reviews in computational chemistry, in: B. Kenny, R.L. Lipkowitz, R.C. Thomas (Eds.), The Poisson–Boltzmann equation, 2003, pp. 147–365.
[36] N.A. Baker, Biomolecular applications of Poisson–Boltzmann methods, in: B. Kenny, R.L. Lipkowitz, R.C. Thomas (Eds.), Reviews in Computational Chemistry, 2005, pp. 349–379.
[37] J. Kottalam, D.A. Case, Langevin modes of macromolecules: applications to crambin and DNA hexamers, Biopolymers 29 (1990) 1409–1421.
[38] H. Gohlke, C. Kiel, D.A. Case, Insights into protein–protein binding by binding free energy calculation and free energy decomposition for the Ras–Raf and Ras–RalGDS complexes, J. Mol. Biol. 330 (2003) 891–913.
[39] V. Zoete, M. Meuwly, M. Karplus, Study of the insulin dimerization: binding free energy calculations and per-residue free energy decomposition, Proteins 61 (2005) 79–93.
[40] O. Aruksakunwong, M. Malaisree, P. Decha, P. Sompornpisut, V. Parasuk, S. Pianwanit, S. Hannongbua, On the lower susceptibility of oseltamivir to influenza neuraminidase subtype N1 than those in N2 and N9, Biophys. J. 92 (2007) 798–807.
[41] M. Malaisree, T. Rungrotmongkol, N. Nunthaboot, O. Aruksakunwong, P. Intharathep, P. Decha, P. Sompornpisut, S. Hannongbua, Source of oseltamivir resistance in avian influenza H5N1 virus with the H274Y mutation, Amino Acids 37 (2009) 725–732.
[42] S. Miyamoto, P.A. Kollman, What determines the strength of noncovalent association of ligands to proteins in aqueous solution? Proc. Natl. Acad. Sci. U.S.A. 90 (1993) 8402–8406.
[43] W. Wang, P.A. Kollman, Free energy calculations on dimer stability of the HIV protease using molecular dynamics and a continuum solvent model, J. Mol. Biol. 303 (2000) 567–582.